**Supplementary Information**

# Optomagnetic nanofluids for controlled brain hyperthermia: A critical study

*Diego Mendez-Gonzalez,[a,b,*] José Lifante,[b,c] Irene Zabala Gutierrez,[a] Riccardo Marin,[c] Erving Ximendes, [b,c,] Elena Sanz-de Diego,[d] M. Carmen Iglesias-de la Cruz,[b,c] Francisco J. Teran,[d,e] Jorge Rubio-Retama [a,b] and Daniel Jaque.[b,c,*]*

*a) Departamento de Química en Ciencias Farmacéuticas, Facultad de Farmacia. Universidad Complutense de Madrid. Plaza Ramon y Cajal 2, Madrid, 28040, Spain*

b) *Nanobiology Group, Instituto Ramón y Cajal de Investigación Sanitaria (IRYCIS), Ctra. De Colmenar Viejo, Km. 9100, Madrid, 28034, Spain*

*c) NanoBIG, Departamento de Física de Materiales, Facultad de Ciencias, Universidad Autónoma de Madrid, C/ Francisco Tomás y Valiente 7, Madrid, 28049, Spain*

*d) IMDEA Nanociencia, Campus Universitario de Cantoblanco, Calle Faraday 9, 28049 Madrid, Spain.*

*e) Nanobiotecnología (IMDEA-Nanociencia), Unidad Asociada al Centro Nacional de*

*Biotecnología (CSIC), 28049 Madrid, Spain*

## I) Materials and methods

### 1) Materials

a) Chemicals

### 2) Methods

a) Synthesis of $Ag_2S$ NPs
b) Surface functionalization of $Ag_2S$ NPs with HS-PEG-$NH_2$
c) Surface functionalization of $Ag_2S$ NPs with HS-PEG-OMe
d) OMNFs ($Ag_2S$ NPs + NFs mixtures)
e) Concentrated mixtures / dispersions for tissue phantom, concentration-dilution effect, viscosity effect, influence of blood plasma and *ex vivo* mouse brain experiments
f) Preparation of tissue phantoms
g) Size and morphological nanoparticle characterization
h) Hydrodynamic size measurements
i) NIR-Visible Absorbance
j) Steady state luminescence
k) Luminescence lifetime measurements
l) Magnetic hyperthermia measurements
m) Magnetometry and SAR calculations
n) Tissue phantom experiments (Scheme S1)
o) In vitro cytotoxicity assays of $Ag_2S$-OMe NPs and NFs
p) Animal handling and sacrifice

q) *Ex vivo* mouse brain experiments

**II) Results**

1) TEM size distribution of magnetic NFs (Figure S1A)
2) DLS size distribution of magnetic NFs (Figure S1B)
3) Extinction spectra of magnetic NFs and $Ag_2S$ NPs in the 500 – 850 range (Figure S1C)
4) Hysteresis loop of magnetic NFs (Figure S1D)
5) TEM size distribution of $Ag_2S$ NPs (Figure S1E)
6) Comparison of HS-PEG(2 kDa)-$NH_2$ and HS-PEG(2 kDa)-OMe as $Ag_2S$ NPs' surface ligand
a) Schematic representation of $Ag_2S$-$NH_2$, $Ag_2S$-OMe NPs and the resulting OMNFs when mixed with magnetic NFs. Optical images of OMNFs' long-term stability (Figure S2A)
b) DLS size distribution of $Ag_2S$-$NH_2$ and $Ag_2S$-OMe NPs (Figure S2B)
c) Luminescence lifetime of $Ag_2S$-$NH_2$ NPs and $Ag_2S$-OMe NPs (Figure S2C)
d) AMF-induced temperature increment produced by NFs alone (control), and by OMNFs (Figure S2D)
e) SAR value of magnetic NFs in the absence and presence of $Ag_2S$-OMe NPs (Figure S2E)

f) Relative luminescence lifetime of $Ag_2S$-$NH_2$ NPs and of $Ag_2S$-PEG-OMe NPs in the presence of increasing concentrations of NFs (Figure S2F)
7) Increase of temperature, as recorded by a thermal and a NIR camera, produced by the optimized OMNF under an AMF (Figure S3A)
8) Overlap of NFs' extinction spectra with the laser excitation and $Ag_2S$-OMe NPs' emission wavelength within the 750-1400 nm range (Figure S3B)
9) Relative thermal sensitivity of $Ag_2S$-OMe in the absence and in the presence of NFs for different temperatures (Figure S3C)
10) Emission intensity change (%) vs temperature of OMNF – Calibration curve. (Figure S4A)
11) DLS size distribution of highly concentrated NFs re-diluted in $H_2O$ and in blood plasma. DLS of blood plasma alone (negative control). (Figure S4B and Table S1)
12) Increase of temperature at the surface of tissue phantom during PTT in the absence of NPs (negative control). (Figure S4C)
13) Increase of temperature produced by 9.4 mg/mL NFs, and by 2.5 mg/mL $Ag_2S$-OMe NPs alone (Figure S4D)
14) Representative local temperature trend during PTT, as calculated from the luminescence intensity of OMNF in a tissue phantom (Figure S5A)
15) Increase of temperature recorded by the thermal camera at the surface of a mouse brain during PTT with 2 µL of OMNF (Figure S5B)
16) Time evolution of local temperature and relative luminescence intensity during consecutive PTT treatments of mouse brain with the OMNF and with $Ag_2S$-OMe alone (Figure S6)
17) In vitro cytotoxicity assays of $Ag_2S$-OMe and magnetic NFs (Figure S7)

**III) References**

## I) MATERIALS & METHODS

### 1) Materials

#### a) Chemicals

Sodium diethyldithiocarbamate (NaDDTC) (ACS reagent grade), silver nitrate (99,9%), oleylamine (70%) (OLA), 1-dodecanethiol (≤98%) (DDT), heterobifunctional HS-PEG(2 kDa)-$NH_2$·HCl, Phosphate buffer saline (PBS), and intralipid (20% emulsion) were purchased from Sigma-Aldrich (Merck). Chloroform ($CHCl_3$) (99.6%) and ethanol absolute pure (99.8%) were purchased from PanReac AppliChem. Blood plasma was obtained from Biowest (FT.S4180an).
Heterobifunctional HS-PEG(2kDa)-Methoxy was purchased from Rapp polymere GmbH.

The magnetic nanoparticles used in this work, Synomag®-D (10 mg/mL aqueous dispersions; dextran $NH_2$ surface coating; 50 nm hydrodynamic diameter), were acquired from ©Micromod Partikeltechnologie GmbH and used as received. These are commercial nanoflower-shaped γ-$Fe_2O_3$ nanoparticles (from now on NFs) whose properties are described in "Results and discussion" Section.

### 2) Methods

#### a) Synthesis of $Ag_2S$ NPs.

The synthesis of the NPs was carried out as previously reported.[1] $Ag_2S$ NPs were synthesized through the thermal decomposition method starting from the precursor silver diethyldithiocarbamate (AgDDTC), previously prepared by the reaction between 0.025 mmol of $AgNO_3$ and 0.025 mmol of NaDDTC, separately pre-dissolved in 200 mL of Milli-Q water. The slowly addition of the NaDDTC solution above the $AgNO_3$ solution produced a yellow precipitate (AgDDTC). The product was filtered under vacuum, dried at 60ºC and stored in a desiccator protected from light for its following use. The production of $Ag_2S$ NPs was carried out by adding 25 mg of AgDDTC (0.1 mmol), 2.5 mL of DDT (10.4 mmol) and 2.5 mL of OLA (7.6 mmol) into a two-neck round-bottom flask at room temperature. The mixture was first sonicated under vacuum for 10 min to remove air and residual water. Subsequently, the mixture was heated up to 185 °C at a heating rate of 20 ºC/min under a nitrogen atmosphere and slow magnetic stirring. The reaction was kept for 1 h and subsequently cooled down naturally. The synthesized NPs were destabilized with 10 mL of ethanol and collected by centrifugation at 10,000 g for 10 min; this process was repeated twice. Finally, the NPs pellet was dispersed in $CHCl_3$ at a concentration of 1 mg/mL and stored at 4 ºC.

#### b) Surface functionalization $Ag_2S$ NPs with HS-PEG-$NH_2$.

3 mL of $Ag_2S$ NPs (1 mg/mL) in $CHCl_3$ were added to a glass vial, subsequently capped, and bath-sonicated until a change in appearance was achieved (from a turbid and colloidally unstable dispersion to a product with high colloidal stability, low scattering, and bright color), typically after 10 min of ultrasonication. Next, the resulting dispersion was added to another vial containing 15 mg of HS-PEG-$NH_2$ (Mw= 2 kDa) and let to incubate for 10 min in an orbital shaker. Then, the NPs were sonicated for 30 s, destabilized through the addition of 6 mL of diethyl ether, and centrifuged at 2000 g for 1 min. The supernatant was discarded, and the resulting pellet was redispersed in 1.5 mL mL of absolute ethanol by manually shaking the vial, and eventually sonicating during ~15 sec. Then, 1.5 mL of di-$H_2O$ was added dropwise to the ethanol dispersion, while the vial was sonicated. The resulting 1/1 ethanol/di-$H_2O$ dispersion was transferred to a 10 mL round bottom flask, and the ethanol and possible $CHCl_3$ traces were removed using a rotary evaporator. The dispersion was then purified using an Amicon 50k centrifuge filter. After 3 cycles of centrifugation and redispersion in di-$H_2O$, the resulting $Ag_2S$-PEG-$NH_2$ NPs were dispersed to a final volume of 40 µL of di-$H_2O$ and stored at 4ºC.

**c) Surface functionalization of $Ag_2S$ NPs with HS-PEG-OMe.**

3 mL of $Ag_2S$ NPs (1 mg/mL) were added to a vial containing 15 mg of HS-PEG-OMe (Mw = 2kDa) and mixed in an orbital shaker for 1h. After this, the dispersion was bath-sonicated until the dispersion changed its appearance, in a similar way as that described for the functionalization of $Ag_2S$ NPs with HS-PEG-$NH_2$, typically after 10 min. The resulting dispersion was then destabilized by the addition of 6 mL of hexane and centrifuged at 2000 g for 1 min. The resulting pellet was redispersed in 1.2 mL of ethanol by hand shaking and eventually sonicating during ~15 sec. After this, 2.8 mL of di-$H_2O$ were added dropwise while sonicating the vial. The solution was next transferred to a 10 mL round bottom flask, and the ethanol and possible $CHCl_3$ traces were removed using a rotary evaporator. The dispersion was then purified using an Amicon 50k centrifuge filter. After 3 cycles of centrifugation and redispersion in di-$H_2O$, the resulting $Ag_2S$-PEG-OMe NPs were dispersed to a final volume of 40 µL of di-$H_2O$ and stored at 4ºC.

**d) OMNFs ($Ag_2S$ NPs + NFs mixtures).**

$Ag_2S$ NPs (with either SH-PEG-$NH_2$ or SH-PEG-OMe as surface functionalization) and NFs where mixed together at different ratios by adding a small volume of $Ag_2S$ NPs (~40 mg/mL), typically a few µL, to a certain volume of commercial NFs (10 mg/mL). di-$H_2O$ was added when necessary to achieve a final volume of 100 µL for each mixture. In this way we were able to test, depending on the case, 5:1, 2.5:1, 2:1, 1.1:1, 1:1, 1:2, 1:3 and 1:3.8 (referred to as ~1:4) $Ag_2S$ NPs + NFs ratios.

**e) Concentrated mixtures / dispersions for tissue phantom, concentration-dilution effect, viscosity effect, influence of blood plasma and *ex vivo* mouse brain experiments.**

Before injection into the tissue phantom (or mouse brain), a volume of optimized OMNFs (i.e. 2.5 mg/mL + $Ag_2S$-OMe NPs + 9.4 mg/mL NFs) was concentrated 3.4-fold by using a centrifuge filter (Amicon 50K), resulting in a final concentration of 40.5 μg/mL. For the injection into the tissue phantom (or mouse brain) of $Ag_2S$-OMe NPs alone, these were pre-concentrated to 20 μg/mL.
In order to prepare the NFs dispersions for the experiments dealing with concentration-dilution, viscosity (80% glycerol), and blood plasma effects on the NFs' SAR value, the commercial dispersion of NFs (10 mg/mL) was concentrated 11-fold to yield a 110 mg/mL NFs stock dispersion from which the dispersions for the corresponding experiments where prepared**.**

**f) Preparation of tissue phantoms**

Fifty mL of di-$H_2O$ were added to a 250 mL Erlenmeyer flask, together with a magnetic stirring bar. Next, the flask was introduced into an oil bath at 90ºC. After 5 min, 625 mg of agar powder were added into the flask, under moderate stirring (700 rpm), along with 2.5 mL of intralipids (20% emulsion). The mixture was kept under stirring at 90ºC for 1h, and then poured into a crystallizing dish and let to cool down to room temperature until the solution gelled. Finally, the gel was unmolded, sliced into pieces of c.a. 430 $mm^3$, and stored in the fridge.

**g) Size and morphological nanoparticle characterization**

The size and morphology of $Ag_2S$ NPs and magnetic NFs were characterized by using a JEOL JEM1400 Flash TEM microscope. Samples were prepared by adding a sample drop on top of formvar-coated copper grids and letting them dry at room temperature.

**h) Hydrodynamic size measurements**

To determine the effective size of $Ag_2S$ NPs and magnetic NFs in $H_2O$ and different solvents, dynamic light scattering (DLS) measurements were performed by using a Zetasizer Nano ZS90 (Malvern Instruments) equipped with a 4.0 mW He−Ne laser operating at 633 nm as energy source, with an angle of 173˚ between the incident beam and the avalanche photodiode detector. To study the agglomeration of NFs, different aqueous media were employed: doubly distilled water (DDW), and blood plasma (75% dilution of commercial blood plasma, 25% PBS 1x) (Biowest, Ref.: FT.S4180an). Nanoparticles samples were diluted in doubly distilled water (DDW) to a final concentration of 0.05 gFe L−1 in a commercial cuvette. The measurements were performed with an automatic scan time, and three scans per measurement.

**i) NIR-Visible Absorbance**

Visible-NIR absorption spectra of the nanoparticles in the range of 500 – 1400 nm were performed with a Perkin Elmer Lambda 1050 spectrophotometer at 1.5 nm step resolution. Quartz cuvettes and micro-cuvettes with 1 cm path were used for the measurements.

**j) Steady state luminescence**

For steady state luminescence measurements, we used a single mode fiber coupled laser diode operating at 808 nm as the excitation source (Lumics BTF14). The laser radiation was first collimated and then focused into the optomagnetic nanofluid by using a fiber collimator (PAF2-A4B from Thorlabs) and a single lens (5 cm of focal length). The luminescence emitted by the dispersion was spectrally analyzed by a fiber coupled spectrometer (Kymera 193i, Andor) with a diffraction grating featuring 75 g/mm and blazed at 1700 nm. The emission was recorded using an InGaAs CCD camera (Andor iDus DU490A). The cuvette containing the nanoparticles was placed in a temperature controlled compact spectrometer sample compartment (QPod 2e™ from Quantum Northwest, Inc.). This allows to change the sample temperature between 10 and 60 $^{o}$C with a temperature accuracy of 0.15 ºC.

**k) Luminescence lifetime measurements**

Luminescence decay curves were acquired by using an Optical Parametric Oscillator (OPO, Lotis TII model LS-2145-OPO) pumped by a frequency tripled Nd:YAG laser operating at 355 nm. The OPO was tuned to 800 nm and provides laser pulses (8 ns duration and 2 mJ energy) with a repetition rate of 10 Hz. The laser radiation was focused into a cuvette containing the optomagnetic nanofluids by using a single lens (5 cm of focal length). The luminescence emitted by the dispersion was collected by a lens (7.5 cm focal length) and sorted by using two long-pass filters (Thorlabs FEL-850) and a monochromator (Kymera 193i). The emitted intensity at 1200 nm was finally detected by an infrared photomultiplier tube with a high sensitivity in the 900-1700 nm range (H10330C from Hamamatsu). The decay profile was then acquired and averaged by a digital oscilloscope (Le Croy Wave Runner). For temperature-controlled measurements, the cuvette containing the nanoparticles was placed in a temperature controlled compact spectrometer sample compartment (QPod 2e™ from Quantum Northwest, Inc.).

**l) Magnetic hyperthermia measurements.**

Magnetic hyperthermia experiments were performed by using a semi-automate equipment for generation of alternating magnetic fields (AC GEN Series, Nanotech Solutions, Spain) with a top optical access of 20×10 mm to the inner cylindrical part of the coil. The value of the field frequency ranges from 45 up to 180 kHz, with a field intensity of 4 to 16 kA/m. A maximum field of 12 kA/m can be used for the maximum frequency (180 kHz). The field intensity varies < 4% along the top-view field region. All magnetic hyperthermia experiments were performed for 5 min. The surface temperature inside the cylinder can be set thanks to a variable cooling bath. The temperature of the optomagnetic nanofluid (within a 500 µL eppendorf tube or a phantom tissue) was monitored by an infrared thermal camera (FLIR E40bx; Thermal

sensitivity <0.045°C or 45 mK). In the cases where NIR luminescence from $Ag_2S$ NPs was recorded during magnetic hyperthermia, an InGaAs SWIR camera (Xenics Xeva 320) equipped with an infrared objective was used to follow the emission intensity evolution during the experiments.

**m) Magnetometry and SAR calculations.**

*AC Magnetometry* measurements of different dispersions containing 9.4 mg/mL NFs alone or in combination with $Ag_2S$ NPs in different media (doubly distilled water, 80% v/v glycerol and blood plasma) were carried out at room temperature under AMFs in the frequency range from 120 up to 240 kHz, with field intensities of 12 kA/m. AC hysteresis loops were obtained with a commercial inductive magnetometer (AC Hyster Advance, Nanotech Solutions, Spain). These magnetic measurements were taken in less than 1 minute. Thus, colloidal stability is maintained during AC magnetization measurements. The values of AC magnetization were normalized to the mass of magnetic elements (i.e. iron). AC hysteresis loop measurements consists in three repetitions to obtain average and standard deviation of the magnetic area values. Afterwards, SAR values were calculated according to $SAR = A \cdot f$, where $A$ is the magnetic area and $f$ is the AC magnetic field frequency.[2]

**n) Tissue phantom experiments.**

Either OMNFs or $Ag_2S$-OMe NPs were injected into the tissue phantom by using a 5 µL Hamilton syringe with a 30-gauge needle. The needle was introduced to a depth of 2.5 mm, after which the selected nanoparticle volume was injected at a flow rate of c.a. 0.2 µL/min. The tissue phantom was then deposited in a glass slide, which was introduced into the coil of the instrument for magnetic hyperthermia. The thermal camera was placed in front of the coil axis, at a distance of 30 cm. An optical setup was built to excite OMNFs or $Ag_2S$-OMe NPs when used as photothermal agents and to record the luminescence of $Ag_2S$ NPs when used as NIR nanothermometers during magnetic hyperthermia or photothermal therapy. This consisted in the use of a diode laser operating at 808 nm used as excitation source (LIMO30-F200-DL808), coupled to a collimator (Thorlabs, PAF2S-5B) with an optical fiber. The collimated beam went towards a long-pass dichroic mirror (Thorlabs, DMLP950) disposed in a 90º angle, to re-direct the beam towards a convergent lens (focal distance = 150 mm) that focused the laser on the surface of the tissue phantom in a spot of 2 mm in diameter. An InGaAs SWIR camera (Xenics Xeva 320) with a Japan Excellent M25.5 objective was placed behind the dichroic mirror, in order to collect the luminescence intensity emitted by the $Ag_2S$-OMe NPs during the experiments. A Thorlabs FEL-850 long-pass filter was placed in front of the SWIR camera sensor to avoid recording laser light reflected from the sample. The data from the SWIR camera allowed for NIR luminescence thermometry of the local temperature generated inside the tissue during the treatments, after proper analyses and comparison with Intensity vs temperature calibration curves. Both magnetic hyperthermia and photothermal therapy experiments were performed for a total time of 5 min.

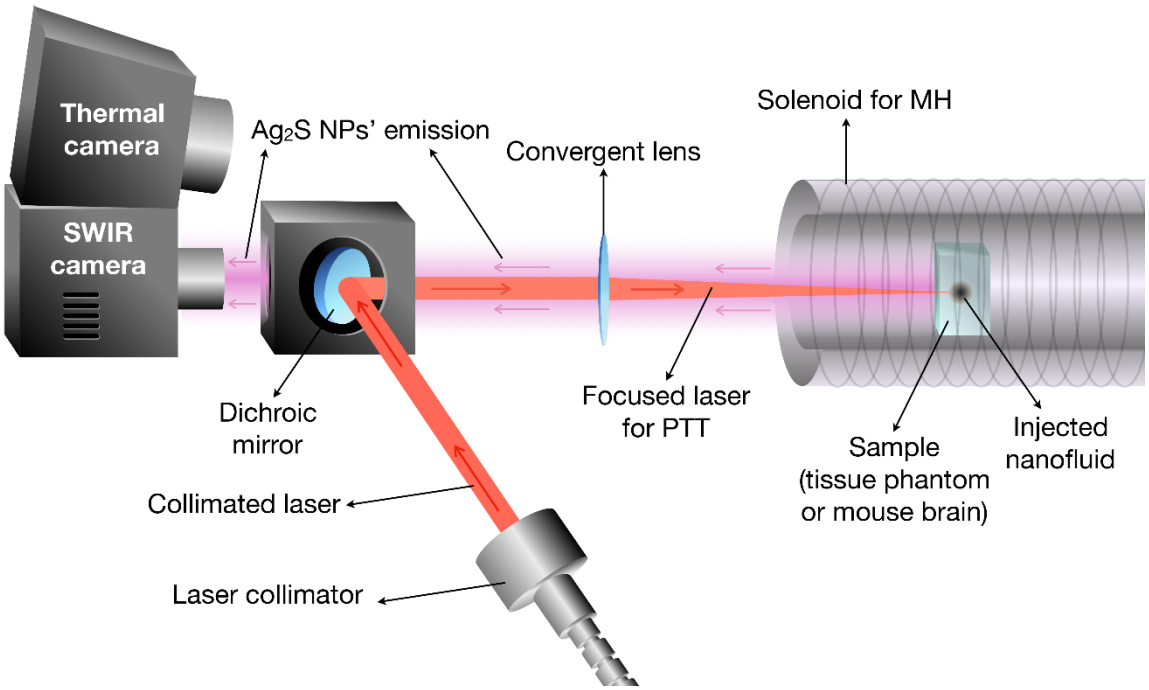


**Scheme S1.** Simplified scheme of the setup used for tissue phantom / mouse brain hyperthermia experiments.

### o) In vitro cytotoxicity assays of $Ag_2S$-OMe NPs and NFs

The determination of the in vitro cytoxicity of $Ag_2S$-OMe NPs and magnetic NFs was performed in a glioblastoma mouse cell line (GL261, (generous gift from Dr. María Abad, Vall D´Hebron Institute of Oncology) by MTT assay. Briefly, cells were grown in DMEM medium (Sigma-Aldrich, USA), supplemented with 10% fetal bovine serum (FBS) (Thermo Fisher Scientific, USA) and a 1% streptomycin– penicillin antibiotic (Sigma-Aldrich, USA). DMEM with FBS and antibiotic is referred hereinafter as complete medium. Upon confluence, GL261 cells were trypsinized, counted using a Neubauer chamber and seeded into 24-well culture plates (at $0.5 \times 10^4$ cells/mL) in complete culture medium (500 µL) for 24 hours. In order to study the effects of the nanoparticles on cell survival, we treated GL261 cells with each type of nanoparticle individually, in a dose range from 2 µg/ml to 50 µg/ml. We performed time-response experiments in all cases, using nanoparticle incubation time points of 6 and 24 hours. After the incubation was finished, culture medium was aspirated and a solution of MTT (Acros Organics™) at 0.5 mg/ml in culture medium was added for 2.5-3 hours in darkness, at 37 ºC and 5% CO2. Once the formazan crystals were evident, the reaction was stopped by carefully aspirating the MTT solution, and crystals were then dissolved by adding DMSO (Fisher Scientific), incubating in darkness at 37ºC and gently shaking for 15 minutes. The optical density (OD) was recorded at 550 nm for every condition. Data from blank wells containing no cells was subtracted to correct for background noise, and cell viability was calculated as:

$$\%\ Cell\ viability = \frac{Abs\ sample}{Abs\ control} \cdot 100$$

### p) Animal handling and sacrifice.

Two different three-month-old male C57/BL6J mice weighting 30 +- 1 gr were used for the *ex vivo* experiments. The animals were sacrificed by beheading under inhaled isoflurane anesthesia (induction 5% Iso 2 L/min $O_2$) after checking total absence of nociceptive response to a limb pitching. The animal was immediately dissected and the brain was harvested to perform the experiments. All *ex vivo* experiments were approved by the regional authority for animal experimentation of the Comunidad de Madrid. These were conducted in agreement to the Universidad Autónoma de Madrid's (UAM) Ethics Committee, in compliance with the European Union directives 63/2021UE and Spanish regulation RD 53/2013.

**q) *Ex vivo* mouse brain experiments.**

OMNFs (2 µL, 81 µg) or $Ag_2S$-OMe NPs (2 µL, 40 µg) were injected into the mouse brain by using a 5 µL Hamilton syringe with a 30-gauge needle. The needle was introduced to a depth of c.a. 2.5 mm, after which the selected nanoparticle volume was injected at a flow rate of approximately 0.2 µL/min. Saline drops were poured onto the brain during the process to avoid dehydration. The brain was subsequently introduced in a home-made compartment filled with saline to prevent dehydration during the experiments. Finally, the brain was irradiated for simultaneous photothermal therapy and NIR luminescence thermometry using a similar setup to that described in "tissue phantom experiments" section. All photothermal therapy treatments were performed at a laser irradiance of 2.3 W/cm$^2$ and a total treatment time of 10 min. Three consecutive photothermal therapy treatments were performed with each sample (OMNF and $Ag_2S$-OMe).

**II) RESULTS**

**1) TEM size distribution of magnetic NFs (Figure S1A)**
**2) DLS size distribution of magnetic NFs (Figure S1B)**
**3) Extinction spectra of magnetic NFs and $Ag_2S$ NPs in the 500 – 850 range (Figure S1C**
**4) Hysteresis loop of magnetic NFs (Figure S1D)**
**5) TEM size distribution of $Ag_2S$ NPs (Figure S1E)**

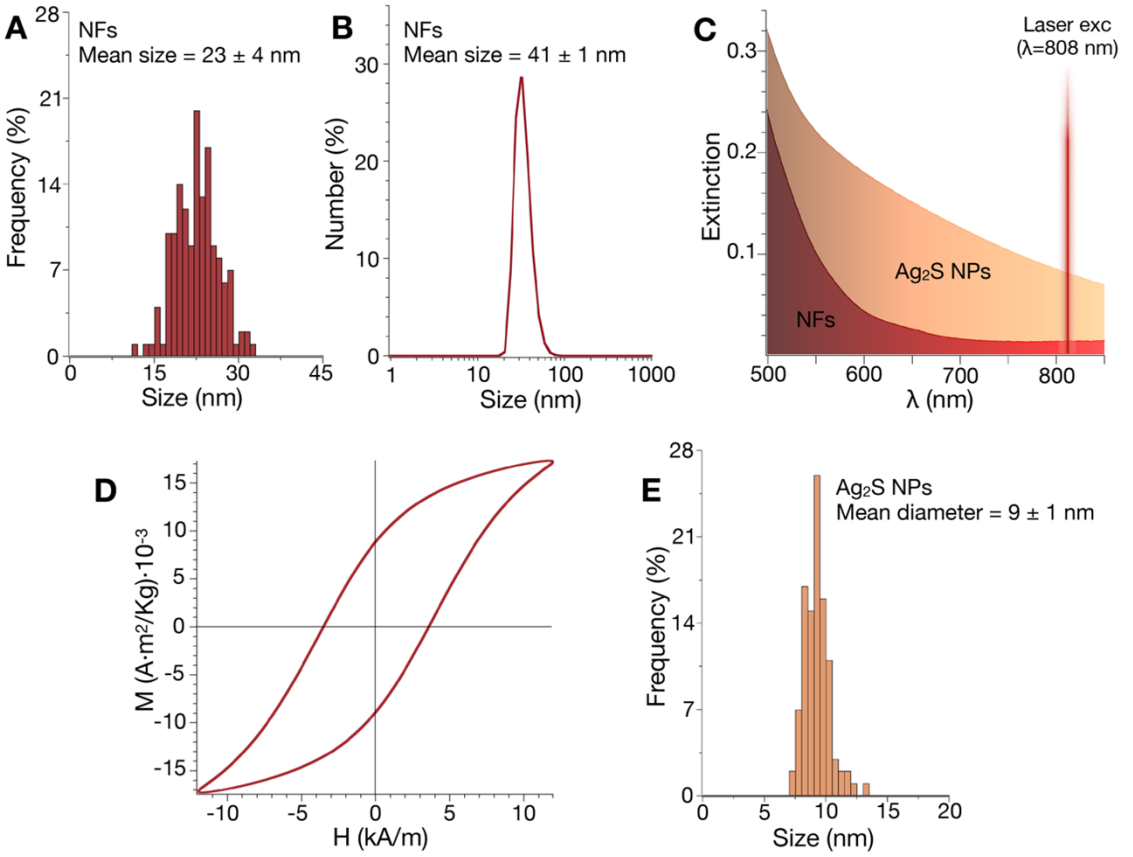


**Figure S1. A.** TEM size distribution of magnetic NFs. Mean diameter is 23 ± 4 nm. **B.** Representative hydrodynamic size distribution of magnetic NFs as obtained by DLS. The mean hydrodynamic diameter for three independent measurements is 41 ± 1 nm. **C.** Extinction spectra of magnetic NFs (red) and $Ag_2S$ NPs (ochre) in the wavelength range of 500 – 850 nm. Spectra were obtained from NFs and $Ag_2S$ NPs dispersions at 0.15 mg/mL. The excitation wavelength (808 nm) used for both PTT and NIR thermometry is included for visual realization of the laser absorption by the NPs. **D.** AC Hysteresis loop as obtained from a 9.4 mg/mL dispersion of NFs in di-$H_2O$ under an AMF of 200 kHz and 12 kA/m. **E.** TEM size distribution of $Ag_2S$ NPs. Mean diameter is 9 ± 1 nm.

**6) Comparison of HS-PEG(2 kDa)-$NH_2$ and HS-PEG(2 kDa)-OMe as $Ag_2S$ NPs' surface ligand (Figures S2A to S2F)**

a) Schematic representation of $Ag_2S$-$NH_2$, $Ag_2S$-OMe NPs and the resulting OMNFs when mixed with magnetic NFs. Optical images of OMNFs' long-term stability (Figure S2A)
b) DLS size distribution of $Ag_2S$-$NH_2$ and $Ag_2S$-OMe NPs (Figure S2B)
c) Luminescence lifetime of $Ag_2S$-$NH_2$ NPs and $Ag_2S$-OMe NPs (Figure S2C)
d) AMF-induced temperature increment produced by NFs alone (control), and by OMNFs (Figure S2D)
e) SAR value of magnetic NFs in the absence and presence of $Ag_2S$-OMe NPs (Figure S2E)
f) Relative luminescence lifetime of $Ag_2S$-$NH_2$ NPs and of $Ag_2S$-PEG-OMe NPs in the presence of increasing concentrations of NFs (Figure S2F)

In order to make possible the fabrication of OMNFs ($Ag_2S$ NPs + NFs), $Ag_2S$ NPs were transferred to water through ligand exchange with polar ligands. Two different hetero-bifunctional polyethylene glycol (PEG) ligands were tested, HS-PEG-$NH_2$ (2 kDa) and HS-PEG-OMe (2 kDa). These ligands were selected as i) the terminal groups (-$NH_2$ and -$OCH_3$, respectively) were expected to minimize the interaction of $Ag_2S$ NPs with the dextran-amino coating of the NFs, and ii) the thiol moiety contained within these molecules presents high affinity towards the surface of the $Ag_2S$ NPs, allowing the replacement of oleylamine (OLA) and 1-dodecanethiol (DDT) capping agents by using a mass excess of ligand. The successful surface modification of $Ag_2S$ NPs yielded $Ag_2S$-PEG-$NH_2$ (from now on $Ag_2S$-$NH_2$), and $Ag_2S$-PEG-OMe (from now on $Ag_2S$-OMe) NPs, respectively, see **Figure S2A**. The resulting dispersions are highly stable in water due to the 2 kDa PEG chains, yielding products of monodisperse size distributions, as proven by the DLS analyses (**Figure S2B**). Interestingly, when comparing the luminescent properties of the $Ag_2S$ NPs with these two functionalizations, notable differences were found. As indicated by the luminescence lifetimes depicted in **Figure S2C**, it can be observed how HS-PEG-OMe (red) resulted in $Ag_2S$ NPs with larger luminescence lifetimes: almost two times compared with those featured by $Ag_2S$-$NH_2$ (brown). The increase in lifetime featured by $Ag_2S$-OMe NPs is ascribed to a better surface coating (i.e. a more closely packed arrangement of the ligands) that can reduce the rate of non-radiative decays assisted by water molecules, and to the absence of amino moieties in the ligand structure, which otherwise can promote non-radiative deexcitation pathways in $Ag_2S$ NPs, as found by our group.[1]

Next, $Ag_2S$-$NH_2$ and $Ag_2S$-OMe NPs were mixed with magnetic NFs in order to determine the influence of their surface functionalization on the optical, magnetic and colloidal properties of the resulting OMNFs. $Ag_2S$ NPs and NFs were initially mixed at 5 mg/mL each (ratio 1:1). This yielded two different OMNFs: $Ag_2S$-$NH_2$ + NFs (ratio 1:1), and $Ag_2S$-OMe + NFs (ratio 1:1). Both mixtures initially resulted in stable colloidal dispersions. Their magnetic heat capacity was examined and compared with that of a dispersion of 5 mg/mL NFs that was used as reference sample (**Figure S2D)**. The temperature increment induced by the control dispersion (NFs only) was found to be $\Delta T$ = 10.5 ºC. In the same AMF conditions, the dispersion containing both NFs and $Ag_2S$-$NH_2$ leads to a temperature increment of $\Delta T$ = 6.7 ºC. This constitutes a 36% decrease in respect to the

control dispersion and indicates that the presence of the $Ag_2S$ NPs reduces the magnetic-induced heating efficiency of NFs. This reduction in the heating efficiency has been also found to depend on the storing time (**Figure S2D**). In fact, one week after the preparation the magnetic field-induced temperature has been further reduced down to ΔT = 3.4 ºC (67.7% decrease) indicating the presence of an undesired dynamic process that reduces the heating efficiency of NFs. This reduction in the heating efficiency is accompanied by an evident long-term tendency to precipitation in the $Ag_2S$-$NH_2$ + NFs OMNF (**Figure S2A-i**). On the other hand, the freshly prepared mixture of $Ag_2S$-OMe with NFs (**Figure S2D**, red bars) yielded a ΔT = 8.7 ºC (i.e. 17% drop in respect to control sample), implying a less pronounced decrease in the magnetic hyperthermal properties of NFs. Interestingly, after one week, the magnetic losses released from the $Ag_2S$-OMe + NFs OMNF remained relatively stable, with a ΔT = 8.4 ºC (20% decrease in respect to control sample). This slight reduction in the heating efficiency has been also confirmed by measuring the SAR value of NFs (9.4 mg/mL) in the presence of $Ag_2S$-OMe NPs (2.5 mg/mL): 188 $W/g_{Fe}$ at f = 180 kHz and H = 12kA/m, which represents c.a. 10% reduction in respect to the SAR of NFs in absence of any $Ag_2S$ NPs (**Figure S2E).** Data included in **Figure S2D** reveals the importance of the chosen surface functionalization of constituent nanoparticles to preserve the colloidal stability, and consequently to maintain the heating efficiency of NFs in the resulting OMNFs. This is explained as NFs agglomeration benefit detrimental magnetic dipolar interactions, which in turn diminish magnetic losses.[3]

In addition, the chosen functionalization has also a profound impact on the luminescent properties of OMNFs. In fact, mixing $Ag_2S$-$NH_2$ with increasing concentrations of NFs drastically shortened $Ag_2S$-$NH_2$'s lifetime (87.5% quenching of photo-luminescence efficiency upon adding 5 mg/mL of NFs, **Figure S2F**, brown). This further confirmed that strong and undesired interactions occur between $Ag_2S$-$NH_2$ and NFs, which are likely responsible for the eventual precipitation observed in **Figure S2A-i**. The exact mechanism behind this quenching cannot be fully identified with the experimental data available. Still, data suggest that it is probably related to surface quenching caused by the interaction of the chemical "$NH_2$" groups from the NFs' amino-dextran surface coating with the surface of $Ag_2S$-$NH_2$ NPs (as similarly reported for these functional groups),[1] due to the latter's inefficient surface passivation. An additional contribution from the nonradiative decay of the excited $Ag_2S$ NPs' through coupling with the electronic levels of magnetic nanoparticles is also expected (i.e. a non-radiative energy transfer process due to the close proximity between NPs, and the overlap between $Ag_2S$ NPs' emission and NFs' absorbance, see **Figure S3B**).[4,5] The undesired chemical interactions between both types of nanoparticles can also explain the reduction of magnetic heating by the NFs and the eventual long-term destabilization and precipitation of the system. As opposed to $Ag_2S$-$NH_2$ NPs, $Ag_2S$-OMe NPs allowed to increase the concentration of NFs within the OMNF up to 9.4 mg/mL, without much affecting their luminescent lifetime c.a. 12% reduction (**Figure S2F, red**). This small

reduction in lifetime may be ascribed to a resonance energy transfer process (RET) that arises due to a reduction in the $Ag_2S$-NFs interparticle distance upon increasing the concentration of NFs (RET acceptor; quencher). Thus, functionalization of $Ag_2S$ NPs with HS-PEG(2 kDa)-OMe seems to avoid undesired chemical interactions with NFs (preventing long-term aggregation; **Figure S2A-ii**), better preserving both the AMF-induced heating capabilities of magnetic NFs and the luminescent properties of $Ag_2S$ NPs. Although a worse surface passivation of $Ag_2S$ NPs using HS-PEG-$NH_2$ may seem counterintuitive in comparison with HS-PEG-OMe, it may be explained by means of a less densely packed arrangement of HS-PEG-$NH_2$. This may be due to the potential interaction of its two functional groups with a single $Ag_2S$ NP, or with two different ones, and also to the different ligand exchange protocol, as ultrasonication in the presence of HS-PEG-$NH_2$ had to be avoided due to its high reactivity, in order to preserve the colloidal properties of $Ag_2S$ NPs. In fact, the reduced luminescence lifetime from the freshly prepared $Ag_2S$-$NH_2$ NPs in comparison with $Ag_2S$-OMe NPs (**Figure S2C**) may suggest that the "$NH_2$ groups" from HS-PEG-$NH_2$ are interacting with the surface of $Ag_2S$ NPs, resulting in a certain degree of luminescence quenching.[1]

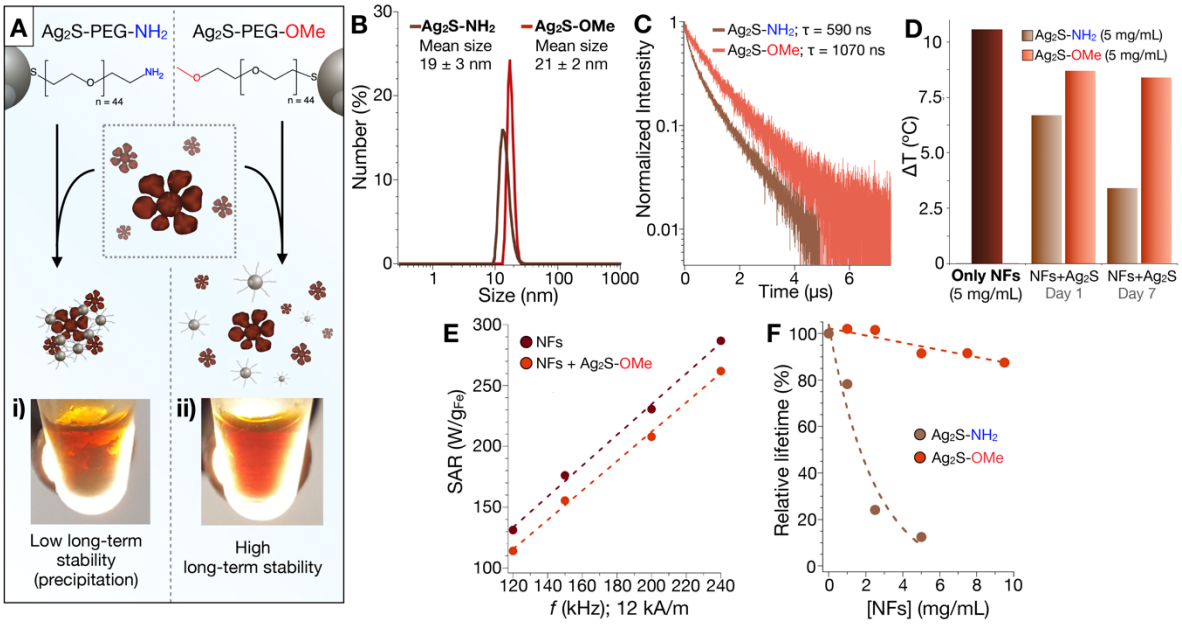


**Figure S2. Properties of functionalized $Ag_2S$ NPs and their mixture with NFs. A.** Schematic representation of the two surface ligands investigated to turn $Ag_2S$ NPs water-dispersible, HS-PEG-$NH_2$ and HS-PEG-OMe. Optical images show **i**) long-term destabilization of mixtures of $Ag_2S$-$NH_2$ NPs + NFs, and **ii**) long-term colloidal stability of $Ag_2S$-OMe NPs + NFs. In both cases, optical images were acquired after 1 month from the preparation of the OMNFs. **B.** Representative size distribution of $Ag_2S$-$NH_2$ NPs (brown) and $Ag_2$-OMe NPs (red) as obtained by DLS. The mean size distribution and standard deviation are the result of three independent measurements. **C.** Luminescence lifetime of $Ag_2S$-$NH_2$ NPs and $Ag_2S$-OMe NPs. Data obtained at room temperature in both cases. **D.** Temperature increment induced under an AMF of 12 kA/m and 180 kHz by a dispersion of 100 µL of NFs alone (5 mg/mL), control, and by 100 µL OMNFs composed by NFs (5 mg/mL) and $Ag_2S$ NPs (5 mg/mL) with either PEG-$NH_2$ (brown bars) or PEG-OMe (red bars) as

surface decoration. Results obtained at day 1 and day 7 after solution preparation are shown for comparison. **E.** SAR ($W/g_{Fe}$) values, as obtained for the magnetic NFs (9.4 mg/mL) in the absence (brown) and in the presence (red) of $Ag_2$-OMe (2.5 mg/mL). Measurements were performed in di-$H_2O$ at 12 kA/m and different *f* (120, 150, 200 and 240 kHz). **F.** Relative luminescence lifetime of 5 mg/mL of $Ag_2S$-$NH_2$ NPs (brown) and 2.5 mg/mL of $Ag_2S$-PEG-OMe NPs (red) in the presence of increasing concentrations of NFs. The relative luminescence lifetimes of $Ag_2S$-$NH_2$ NPs and $Ag_2S$-OMe NPs have been normalized (100%) to their value in the absence of NFs.

**7) Increase of temperature, as recorded by a thermal and a NIR camera, produced by the optimized OMNF under an AMF (Figure S3A)**
**8) Overlap of NFs' extinction spectra with the laser excitation and $Ag_2S$-OMe NPs' emission wavelength within the 750-1400 nm range (Figure S3B).**
**9) Relative thermal sensitivity of $Ag_2S$-OMe in the absence and in the presence of NFs for different temperatures (Figure S3C)**

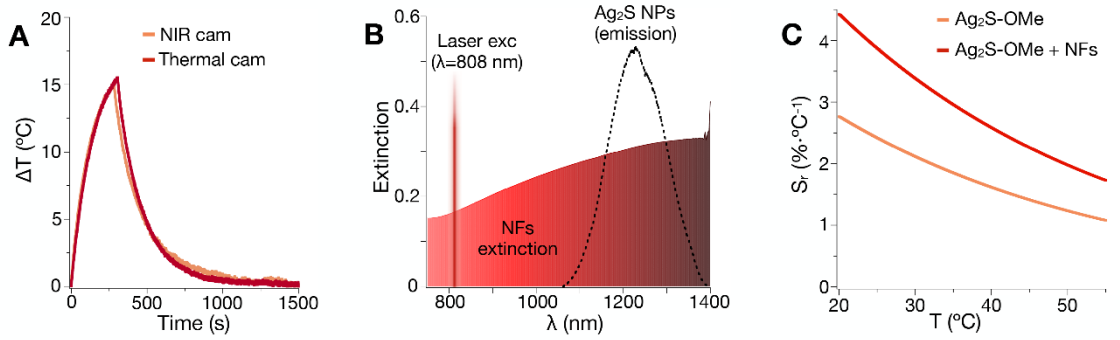


**Figure S3. A.** Temperature increase produced by 100 µL of a dispersion of 9.4 mg/mL NFs + 2.5 mg/mL $Ag_2S$-OMe NPs under an AMF of 12 kA/m and 180 kHz, as obtained from the thermal camera (dark red) and by NIR luminescence thermometry (ochre). The dispersion was contained in an 0.5 mL eppendorf tube during the experiment. **B.** Extinction spectra from magnetic NFs (1 mg/mL) in the 750-1400 nm wavelength range. Laser excitation and $Ag_2S$-OMe NPs' emission spectra are included to show the overlap with the NF's extinction spectra. This overlap confirms the presence of an important inner filter effect that will influence both the excitation of $Ag_2S$-OMe NPs as well as their detected emission. **C.** Relative thermal sensitivity ($S_r$), as obtained from the relative intensity curves in **Figure 2D**, of $Ag_2S$-OMe (2.5 mg/mL) in the absence (ochre) and in the presence (red) of magnetic NFs (9.4 mg/mL) for different temperatures. The change in the relative thermal sensitivity is evident after the addition of magnetic NFs. Relative thermal sensitivity is calculated as found elsewhere,[6] and is defined as:

$$S_r = \frac{1}{\Delta}\left|\frac{\partial \Delta}{\partial T}\right|$$

Where "Δ" represents the thermometric parameter that is studied (e.g. emission intensity, in our case), and "$\left|\frac{\partial \Delta}{\partial T}\right|$" represents the rate of change of the thermometric parameter with temperature. The resulting relative sensitivity is expressed in the plot as "% Intensity change · ºC$^{-1}$".

**10) Emission intensity change (%) vs temperature of OMNF – Calibration curve. (Figure**

**S4A)**

**11) DLS size distribution of highly concentrated NFs re-diluted in $H_2O$ and in blood plasma. DLS of blood plasma alone (negative control). (Figure S4B and Table S1)**

**12) Increase of temperature at the surface of tissue phantom during PTT in the absence of NPs (negative control). (Figure S4C)**

**13) Increase of temperature produced by 9.4 mg/mL NFs, and by 2.5 mg/mL $Ag_2S$-OMe NPs alone (Figure S4D)**

**Figure S4. A.** Calibration curve of OMNFs depicting the % change in luminescence intensity vs

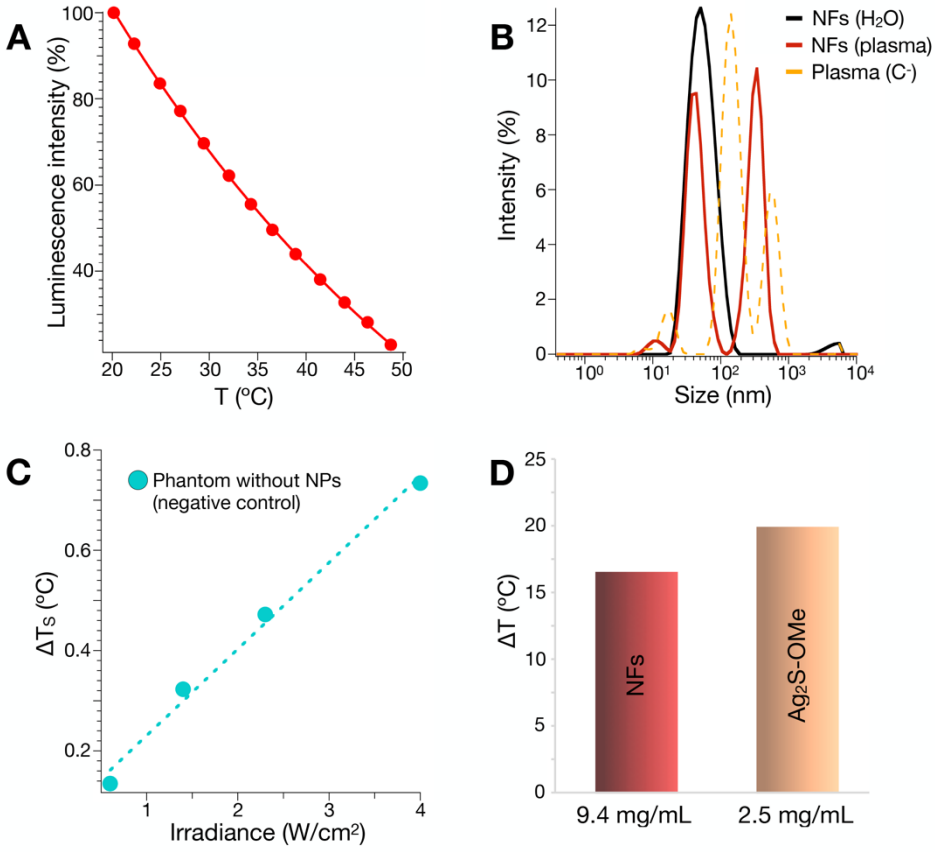


temperature. **B.** Hydrodynamic size as obtained from DLS measurements of highly concentrated NFs when I) re-diluted in $H_2O$ (black), or ii) re-diluted in blood plasma (red). Hydrodynamic size of blood plasma alone (orange) is depicted for comparison, as negative control, showing the size distribution of its constituents (e.g. plasma proteins). DLS analyses confirm that the dilution in $H_2O$ of pre-concentrated NFs results in partially agglomerated products (see hydrodynamic size of original NFs in $H_2O$ in Figure S1B for comparison). DLS analyses of NFs diluted in blood plasma (red) confirm that further agglomeration occurs in this media giving rise to a new peak (population) of larger sizes (> 100 nm). **C.** Temperature increase of the tissue phantom surface as recorded by the thermal camera for different irradiances (0.6, 1.4, 2.3 and 4 W/cm$^2$) in the absence of NPs (negative control). Laser beam diameter is 2 mm. **D.** Temperature increase produced by a dispersion containing 9.4 mg/mL of NFs (red), and by a dispersion containing 2.5 mg/mL $Ag_2S$-OMe NPs. During the experiments, the dispersions were in an eppendorf tube. Temperature was recorded with a thermal camera.

**Table S1**: Intensity-weighted hydrodynamic sizes and standard deviations obtained from DLS measurements of the studied nanoparticles dispersed in different media.

| **Sample** | ***Medium*** | ***Hydrodynamic size*, nm** | ***PDI*** |
|---|---|---|---|
| NFs | $H_2O$ | 49 | 0.18 |
| NFs | Blood plasma | 220 | 0.4 |

**14) Representative local temperature trend during PTT, as calculated from the luminescence intensity of OMNF in a tissue phantom (Figure S5A)**
**15) Increase of temperature recorded by the thermal camera at the surface of a mouse brain during PTT with 2 µL of OMNF (Figure S5B)**

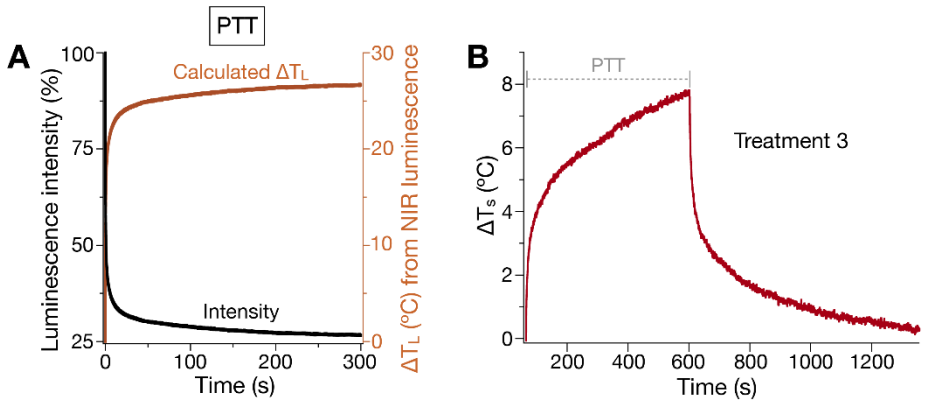


**Figure S5. A.** Representative local temperature trend (ochre scale, right) during PTT (2.3 W/cm2) of 2 µL of OMNF (81 µg), as calculated from the relative luminescence intensity variation (black scale, left). Injection was performed in a tissue phantom. **B.** Surface temperature increase during PTT (2.3 W/cm$^2$) generated by a 2 µL injection of OMNF (81 µg) into a mouse brain, as recorded by the thermal camera.

**16) Time evolution of local temperature and relative luminescence intensity during consecutive PTT treatments of mouse brain with the OMNF and with $Ag_2S$-OMe alone (Figure S6)**

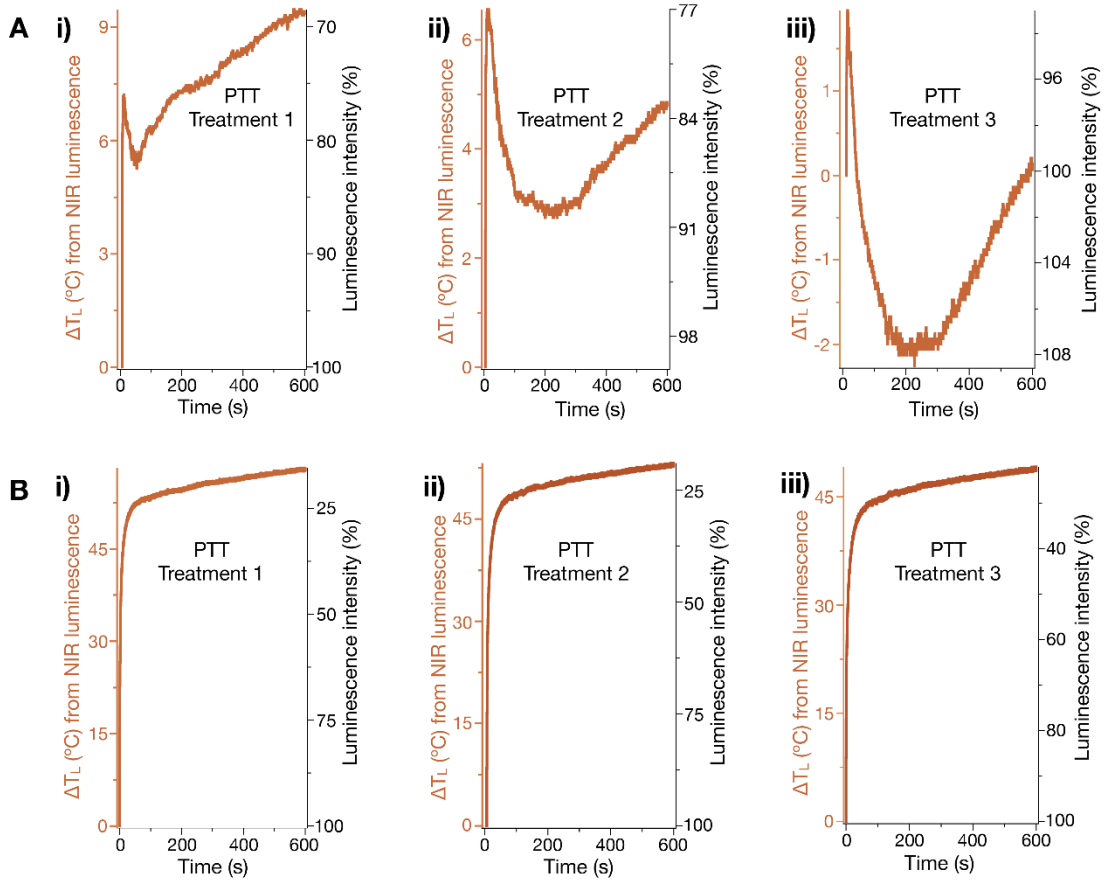


**Figure S6. A.** Time evolution of the local temperature (ochre scale, right) and the relative luminescence intensity (black scale, right) as obtained for 2 µL of OMNF (81 µg) during three consecutive PTT treatments of mouse brain (i, ii and iii, respectively; 2.3 W/cm$^2$, 10 min). **B.** Time evolution of the local temperature (ochre scale, right) and the relative luminescence intensity (black scale, right) as obtained for 2 µL of $Ag_2S$-OMe alone (40 µg) during three consecutive PTT treatments of mouse brain (i, ii and iii, respectively; 2.3 W/cm$^2$, 10 min).

**17) In vitro cytotoxicity assays of $Ag_2S$-OMe and magnetic NFs (Figure S7)**

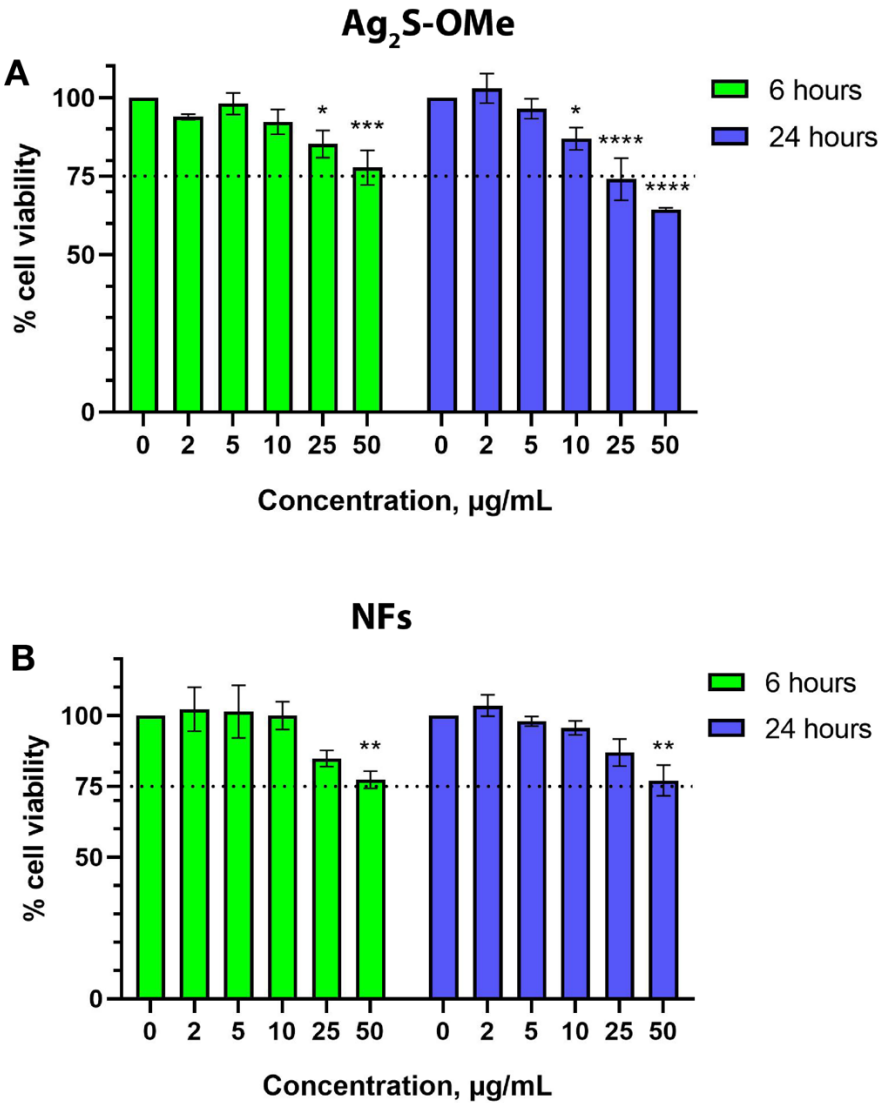


**Figure S7.** Cytotoxicity assessment for **A.** Ag2S-OMe NPs and **B.** Magnetic NFs. GL261 cells were incubated with increasing concentrations of either Ag2S-OMe NPs or NFs for 6 and 24 hours. Then, a MTT assay was performed. Data is represented as mean ± SEM of N=4 replicates. All data were compared with the control (ANOVA test corrected with Dunnett´s test, * $p<0.033$, **$p<0.002$, *** $p< 0.0002$, **** $p<0.0001$).

## III) REFERENCES


1. Gutierrez, I. Z. *et al.* Boosting the Near-Infrared Emission of Ag2S Nanoparticles by a Controllable Surface Treatment for Bioimaging Applications. *ACS Applied Materials & Interfaces* **14**, 4871–4881 (2022).

2. Mehdaoui, B. *et al.* Influence of a transverse static magnetic field on the magnetic hyperthermia properties and high-frequency hysteresis loops of ferromagnetic FeCo nanoparticles. *Applied Physics Letters* **100**, 052403 (2012).

3. Ovejero, J. G. *et al.* Effects of inter- and intra-aggregate magnetic dipolar interactions on the magnetic heating efficiency of iron oxide nanoparticles. *Physical Chemistry Chemical Physics* **18**, 10954–10963 (2016).

4. de Melo, F. M., Grasseschi, D., Brandão, B. B. N. S., Fu, Y. & Toma, H. E. Superparamagnetic Maghemite-Based CdTe Quantum Dots as Efficient Hybrid Nanoprobes for Water-Bath Magnetic Particle Inspection. *ACS Applied Nano Materials* **1**, 2858–2868 (2018).

5. Melle, S. *et al.* Förster Resonance Energy Transfer Distance Dependence from Upconverting Nanoparticles to Quantum Dots. *The Journal of Physical Chemistry C* **122**, 18751–18758 (2018).

6. Brites, C. D. S., Balabhadra, S. & Carlos, L. D. Lanthanide-Based Thermometers: At the Cutting-Edge of Luminescence Thermometry. *Advanced Optical Materials* **7**, 1801239 (2019).